Quantum Simulation

an introduction

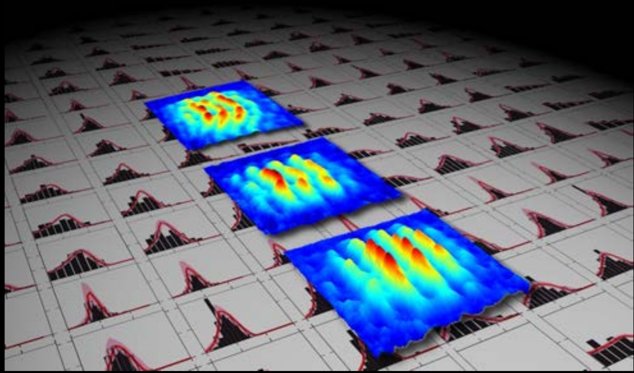

Jörg Schmiedmayer

Vienna Center for Quantum Science and Technology, TU-Wien

ISOQUANT SFB1225

erc

Outline

Lecture 1: Introduction

- Simulating physics with computers -> Quantum simulation
- Basic concepts

Lecture 2: Examples

- Analog quantum simulation
- Digital quantum simulation

Lecture 3: Simulating quantum fields in the lab

- Relativisitc quantum fields
- Emergent Sine-Gordon quantum simulator

Outline

Lecture 2: Implemementing Quantum Simulations

- Quantum Simulation – an overview
  - Scientific opportunities
  - Platforms
  - Challenges
  - Verification
- Analog quantum simulation
  - Atoms in optical lattices
  - Hubbard Model
  - Mott-insulator phase transition
  - Tools
  - Examples (tutorial: Fermi Hubbard model – anti ferromagnet)
- Digital quantum simulation
  - Ion trap digital quantum simulation
  - Examples (tutorial: lattice gauge theory)

Quantum Simulation

Digital Quantum Simulators:

Trotter-Suzuki's decomposition of the many-body evolution operator into sequences of of elementary quantum gates.

Example: *Real-time dynamics of lattice gauge theories with a few-qubit quantum computer*
E. A. Martinez et al. Nature **534**, 516 (2016)

Analog Quantum Simulators:

Build the desired Hamiltonian directly in the Lab and prepare the ground state, observe time evolution.

Example: Hubbard Model, … *Quantum simulation with ultracold atomic gases,*
I. Bloch, et al. Nature Phys. 8, 267 (2012).

Emergent Quantum Simulators (lecture III)

The complexity of the many body wave function does not allow to 'observe' all the details. Every measurement we do is a 'coarse graining' which leads to an emerging effective description that is very different from the microscopic physics.

Example: Sine-Gordon model <-> two tunnel coupled superfluids

Schweigler , et al. Nature **545**, 323 (2017)
Zache et al. arXiv:1909.12815.

Scientific Opportunities for Quantum Simulators

Quantum simulators: Architectures and Opportunities,
E. Altman et al., PRX-Quantum **2**, 017003 (2021).

1. **Quantum materials**
   correlated electronic materials, high temperature superconductors,
   frustrated quantum magnets, spin ice, spin glass
   Bose-Hubbard, Fermi-Hubbard model QuSim: -> explore exotic phases
2. **Quantum chemistry**
   calculation excitation rates, modelling catalysis … , nitrogen fixation, light harvesting
   emulating models of reactions and molecules
3. **Quantum devices and transport**
   calculation quantum properties of (nanoscale) electronic devices
   transport of spin, current, heat, information, … quantum networks of devices
4. **Gravity, particle physics and cosmology**
   lattice gauge theories, color superconductivity, defect formation, curved space time, horizons,
   Unruh radiation, …. many body quantum chaos and scrambling
5. **Non equilibrium many body dynamics**
   spans all scales, really hard problems that can not be traced on classical computers
   from relaxation and thermalization -> emergence of classical world

Platforms for Quantum Simulation

Quantum simulators: Architectures and Opportunities,
E. Altman et al., PRX-Quantum **2**, 017003 (2021).

- **Cold and ultracold molecules** — rich internal structure, 'long range' dipole-dipole interactions for polar molecules
- **Color centers** — Very many incarnations, NV-center in diamond, 'artificial' atoms, long coherence time, fixed in solid but inhomogeneous broadening
- **Dopants in semi conductors** — Very many incarnations, 'artificial' atoms, fixed in solid but inhomogeneous broadening
- **Gate defined quantum dots** — Flexible design, coherence time is an issue of material purity, recently big breakthroughs due t spin-0 hosts (^{28}Si)
- **Photons in nano structures** — Mature technology, but problem with loss and detection that needs to be overcome, mostly probabilistic
- **Photons and atoms in cavities** — Light in cavity mediates long range interaction, exciting developments when combining with singles site detection/manipulation
- **Rydberg atom arrays** — controllable strong interaction, fast loading and operation time, reusable samples, easily scalable, arbitrary arrangements
- **Superconducting quantum circuits** — Designed nodes (qubits) and designed connections. very fast (ns operation time), need exquisite fine tuning, ideal for disorder physics
- **Trapped atomic ions** — System with the best and most robust control, long coherence, difficult to scale up, digital quantum gate based quantum simulation
- **Ultra cold neutral atoms** — Best isolation from environment, 100 thousand's identical nodes, wel ldeveloped techniques to cool, control, measure, bosons <-> fermions
- **Van der Waals heterostructures, Moire materials, Exciton – Polariton, quantum fluids of light** — Many new possibilities. Excitons and quantum fluids of light allow to simulate driven dissipative systems

Challenges

Quantum simulators: Architectures and Opportunities,
E. Altman et al., PRX-Quantum **2**, 017003 (2021).

1. **Scalability and complexity**
   variability of the constituents <-> control
   connectivity <-> complexity
   operation speed <-> isolation and coherence
2. **State preparation and control**
   how to prepare the initial states: complexity <-> cooling
   error propagation <-> engineered baths
   optimal quantum control …
3. **Verification of simulators**
   how can I know if my simulator does what it is supposed to do?
4. **Readout**
   how to read a simulator, how to read a complex wave function
   one can not do tomography (exponential difficult)
   correlation functions become very hard to analyse for non trivial (correlated) systems

Verifying Quantum Simulation

Quantum simulators: Architectures and Opportunities,
E. Altman et al., PRX-Quantum **2**, 017003 (2021).

1. **Validating analog quantum simulators**
   systems contain contributions to Hamiltonian that are not related to the model to be simulated
   universality of low energy physics may save the simulation
   quantification of the different perturbations and their effect on the simulation is mostly unknown
2. **Validating digital quantum simulators**
   digitization errors, Trotter step errors, control errors on gates … de-coherence
   tools exist for small scale systems (<10 qubits) … need benchmarking tools that work for large systems
3. **Comparison to classical calculation**
   limited to cases where there are classical algorithms for some parameter space of the simulation
4. **Verification of simulators**
   run simulation a different systems, self verification, …. new methods in the works
5. **Error correction and mitigation**
   identify and correct for unwanted interactions … especially important for analog QuSim
6. **Mesoscopic metric for quantum complexity**
   models based on asymptotic limits … but real systems are finite and mesoscopic

Analog Quantum Simulation

Build the desired Hamiltonian directly in the Lab and prepare the ground state, observe time evolution, … .

Example:
- Hubbard Model
- Lieb-Lininger Model
  Fermi-Hubbard antiferromagnet
- Disorder physics,
- MBL
- …

Question:
- how good does one need to control the parameters?
- how to verify the results
- …

Main platforms:

- Ultra cold atoms
  - Bosons <-> Fermions
  - Lattices <-> continouse systems
  - Atoms are identical ☺
  - Slow ($t_{op} \sim$ ms) t_{coh} / t_{op} ~ 10^5
  - Experiment cycle time $>$ seconds
- Rydberg atoms in optical tweezers
  - Atoms are identical ☺ Bosons <-> Fermions,
  - Arbitrary designed configurations
  - Not only next neighbor interactions
  - Faster ($t_{op} \sim \mu$s) t_{coh} / t_{op} ~ 10^5
  - Experiment cycle time $> 10^{-3}$ seconds
- Superconducting circuits
  - Designed nodes and connectivity
  - Local control of node and connections
  - Needs fine tuning
  - Fast ($t_{op} \sim$ ns) t_{coh} / t_{op} ~ 10^5
  - Experiment cycle time $> 10^{-6}$ seconds

Analog Quantum Simulation

Build the desired Hamiltonian directly in the Lab and prepare the ground state, observe time evolution, … .

Quantum simulation with ultracold atomic gases, I. Bloch, J. Dalibard, S. Nascimbène, Nature Phys. 8, 267 (2012).

Example:
- Hubbard Model
- Lieb-Lininger Model
  Fermi-Hubbard antiferromagnet
- Disorder physics,
  MBL
- …

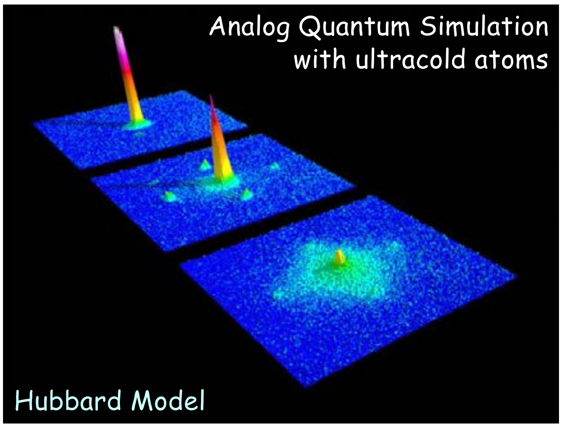

Question:
- how good does one need to control the parameters?
- how to verify the results
- …

Optical Lattices

periodic potentials to trap and manipulate atoms

Trapping Atoms in Light Fields
Optical Dipole Potentials

Energy of a dipole in an electric field: $U_{dip} = -\vec{d} \cdot \vec{E}$

electric field induces a dipole moment: $\vec{d} = \alpha \vec{E}$

Dipole potential: $U_{dip} \propto -\alpha(\omega) I(\vec{r})$

Complex optical potetnial: $V_{Opt} = \hbar \dfrac{\Omega_{Rabi}^2}{4\Delta + i2\Gamma}$

couppling $\hbar\Omega_{Rabi} = d_e E$

detuning $\Delta = \omega_{Laser} - \omega_{Atom}$

decay rate Γ

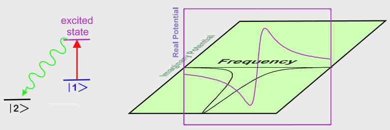

Blue detuning:

Atoms repelled from intensity maxima

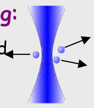

Red detuning:

Atoms trapped in intensity maxima

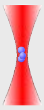

For a review see R. Grimm et al.
Adv. At. Mol. Opt. Phys. 42, 95-170 (2000).

1 D

mirror

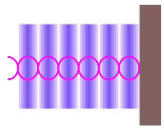

For large detuning

$$U(x) = \frac{\hbar\Omega_0^{\,2}}{4\Delta}\left(1 + \cos(\vec{G}\vec{x} + \delta_0)\right)$$

2 D

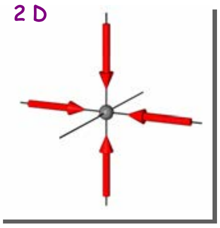

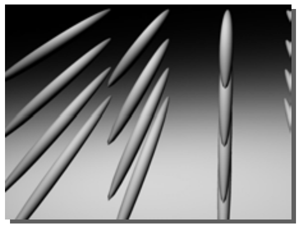

3 D

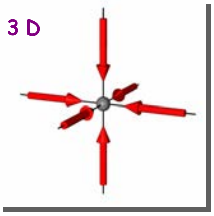

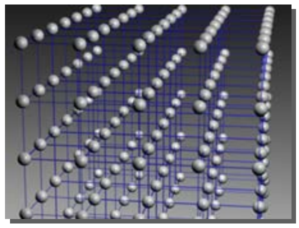

2 beam lattice

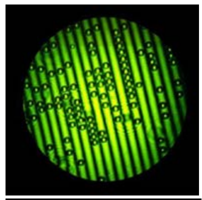

4 beam lattice

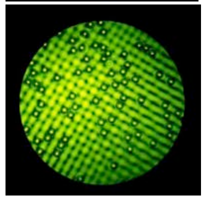

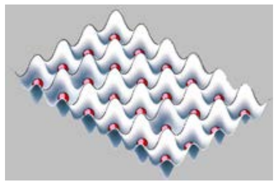

Crystalline solids

How to build a lattice

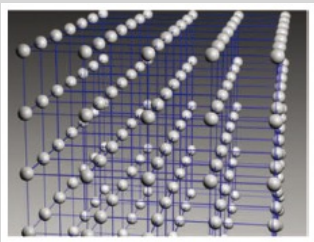

The Bose-Hubbard model

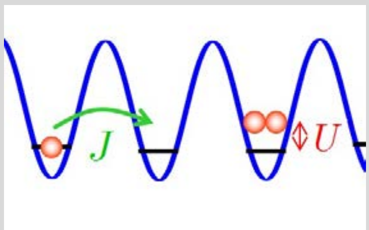

Superfluid to Mott insulator

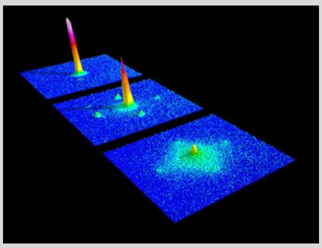

Quantum gas microscope

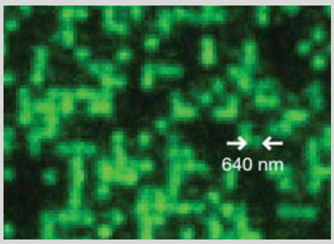

Optical Lattices

$$V(\vec{r}) = V_{0x}\cos^2(k_x x) + V_{0y}\cos^2(k_y y) + V_{0z}\cos^2(k_z z)$$
+ weak harmonic confinement

- the resulting potential is a simple cubic lattice
- the lattice potential is perfect: no defects, no slips
- the BEC coherently spreads over more than 100.000 lattice sites
- filling per site: 1-3 atoms
- potential depth can be adjusted between 0..50 E_{recoil}
- trap frequency per site ≈ 2π x 50 kHz
- energy scale: $E_{recoil} = \dfrac{\hbar^2 k^2}{2m}$
- confinement $\omega_T = \sqrt{4 V_0 E_{recoil}}$ $\quad a_0 = \sqrt{1/\omega_T}$

Optical Dipole Forces

Optical lattice:

4 µm polystyrol particles on water surface

conservative light force for macroscopic particles → optical tweezers

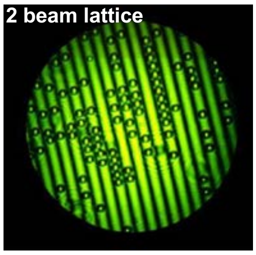

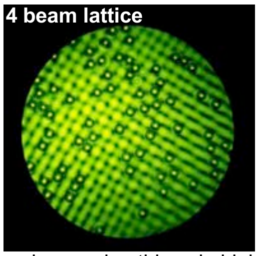

optical tweezers do amazing things in biology (measure the force of a ribosome)

Optical Lattices

$$V(\vec{r}) = V_{0x}\cos^2(k_x x) + V_{0y}\cos^2(k_y y) + V_{0z}\cos^2(k_z z)$$
+ weak harmonic confinement

- the resulting potential is a simple cubic lattice
- the lattice potential is perfect: no defects, no slips
- the BEC coherently spreads over more than 100.000 lattice sites
- filling per site: 1-3 atoms
- potential depth can be adjusted between 0..50 E_{recoil}
- trap frequency per site ≈ 2π x 50 kHz
- energy scale: $E_{recoil} = \dfrac{\hbar^2 k^2}{2m}$
- confinement $\omega_T = \sqrt{4 V_0 E_{recoil}}$ $\quad a_0 = \sqrt{1/\omega_T}$

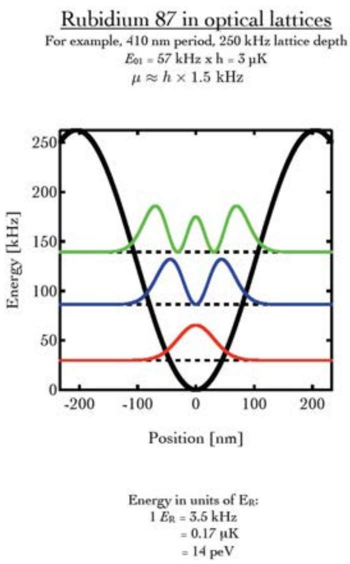

lattice physics: bloch bands

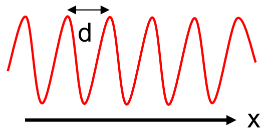

$$K = \frac{2\pi}{d}$$

Ansatz: periodic Bloch waves

$$\boxed{\Psi_q(x) = u_q(x) e^{iqx/\hbar}}$$

with $u_q(x) = u_q(x+d)$ so that $\Psi(x+d) = \Psi(x) e^{iqd/\hbar}$

q is called **quasimomentum** and gives the phase difference between lattice sites

$u_q(x)$ is periodic in K, it can be expressed as $u_q(x) = \sum_n c_{n,q} e^{inKx}$ decomposition in plain waves

$$\boxed{\Psi_q(x) = \sum_n c_{n,q} e^{i(q/\hbar + nK)x}}$$

$\Psi_q(x)$ has discrete momentum komponents $q + n\hbar K$ separated by the reciprocal lattice vector
band structure

double well

many wells

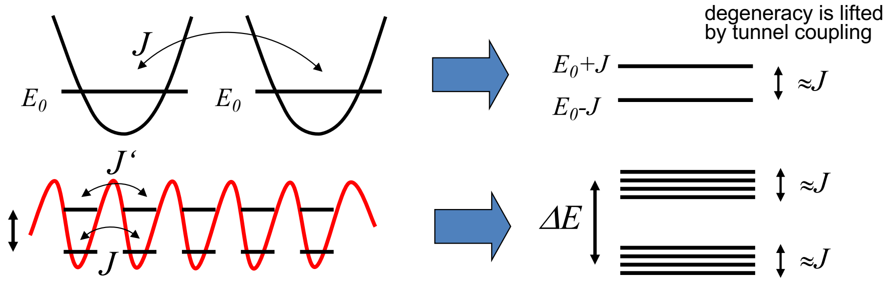

For a quasi infinite lattice, we expect the appearence of a **band structure**

lattice physics: bloch bands
first Brillouin zone representation

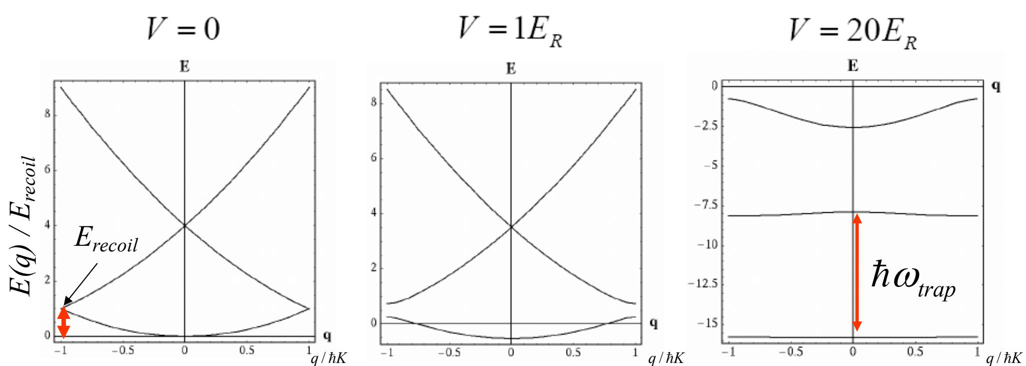

free particle parabola | gapped excitation spectrum | vibrational states in the lattice

$$H = \frac{p^2}{2m} + \frac{V}{2}\cos Kx$$

looking for E(q) such that $H\Psi_q = E(q)\Psi_q$

solving the Hamiltonian for each quasimomentum using the $|q+n\hbar K\rangle$ basis:

$$\frac{(q+n\hbar K)^2}{2m} c_n + \frac{V}{4} c_{n+1} + \frac{V}{4} c_{n-1} = E(q) c_n$$

which has to be solved numerically for each n and q

Result: **Bloch bands**

A typical lattice experiment

…the „Greiner / Bloch machine“…
now working on more than 10 labs

Atomic Species	^{87}Rb
Wavelength	830-850 nm
Waist (1/e²)	125 µm
Polarization	Orthogonal between standing wave pairs
Intensity control	All beams intensity stabilized
Lattice geometry	Simple cubic
Lattice spacing	425 nm

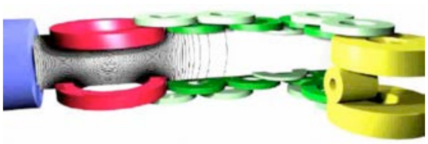

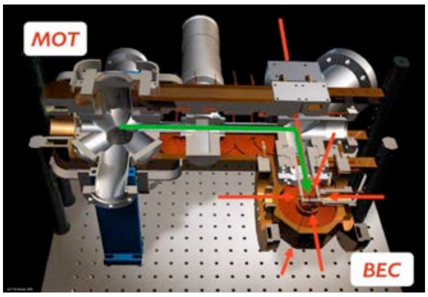

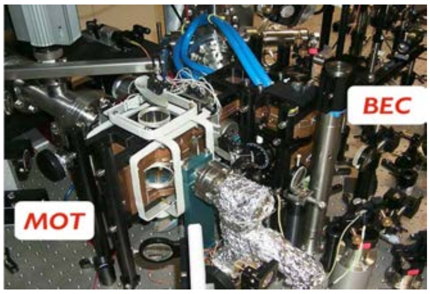

BEC in an Optical Lattice
Matter Wave Interference

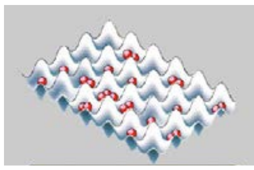

BEC in lattice:

$$\Psi(x) = \sum_j A(x_j) \cdot w(x - x_j) \cdot e^{i\phi(x_j)}$$

Number of atoms on jth lattice site — Localized wave function on Jth lattice site — Phase of wave function on jth lattice site

start with a pure condensate in a magnetic trap

turn on lattice potential adiabatically, so that the wave function remains in the many body ground state of the system!

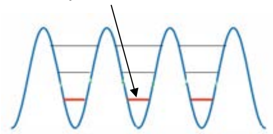

Momentum Distributions 1D diffraction

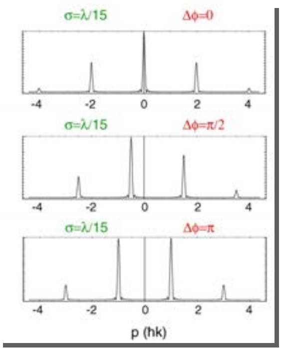

Adjusting the phase difference between neighboring lattice sites

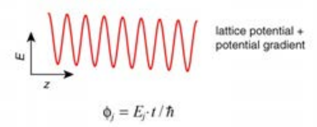

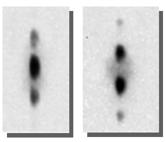

Phase difference between neighboring lattice sites

$\Delta\phi_j = (V'\lambda/2) \cdot t/\hbar$

$\Delta\phi = 0$ $\Delta\phi = \pi$

Time of flight experiment 3D lattice

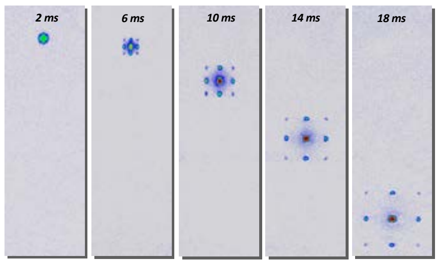

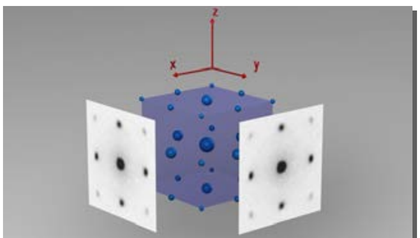

Individual condensates in the lattice expand and interfere with each other, revealing the momentum distribution of the atoms in the lattice.

Bose-Hubbard Model

take into account interactions between particles ocupying the same site

$$H = -J\sum_{i,j}\hat{a}_i^{+}\hat{a}_j + \frac{1}{2}U\sum\hat{n}_i(\hat{n}_i - 1)$$

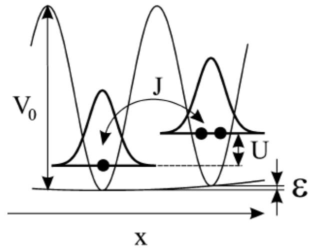

Tunneling term:

J: tunneling matrix element

$\hat{a}_i^\dagger \hat{a}_j$: tunneling from site j to site i

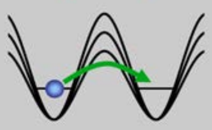

Interaction term:

U : on-site interaction matrix element

$\hat{n}_i(\hat{n}_i - 1)$: n atoms collide with n-1 atoms on same site

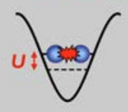

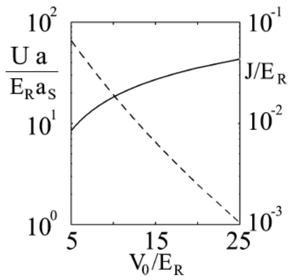

the ratio between **tunelling J** and **interaction U** can be varied by changing the depth of the 3D lattice potential

In 1998, D. Jaksch and P. Zoller proposed to observe the **superfluid – Mott insulator transition** using bosons in optical lattices (never observed in solid state system)

Bose-Hubbard Model

M.P.A. Fisher et al, PRB 40, 546 (1989)
D. Jaksch et al., PRL 81, 3108 (1998)

Expanding the field operator in the Wannier basis of localized wave functions on each lattice site, yields :

$$\hat{\psi}(\boldsymbol{x}) = \sum_i \hat{a}_i w(\boldsymbol{x} - \boldsymbol{x}_i)$$

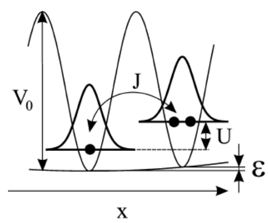

Bose-Hubbard Hamiltonian

$$H = -J\sum_{\langle i,j\rangle}\hat{a}_i^\dagger\hat{a}_j + \sum_i \varepsilon_i\hat{n}_i + \frac{1}{2}U\sum_i\hat{n}_i(\hat{n}_i - 1)$$

Tunnelmatrix element/Hopping element

$$J = -\int d^3x\, w(\boldsymbol{x} - \boldsymbol{x}_i)\left(-\frac{\hbar^2}{2m}\nabla^2 + V_{lat}(\boldsymbol{x})\right)w(\boldsymbol{x} - \boldsymbol{x}_j)$$

On-site interaction matrix element

$$U = \frac{4\pi\hbar^2 a}{m}\int d^3x\,|w(\boldsymbol{x})|^4$$

Superfluid Limit

Tunneling matrix element dominates

Atoms are delocalized over the entire lattice !
Macroscopic wave function describes this state very well.

$$|\Psi_{SF}\rangle \propto \left(\sum_{i=1}^{M}\hat{a}_i^\dagger\right)^N|0\rangle \qquad \langle a_i\rangle \neq 0$$

Poissonian atom number distribution per lattice site

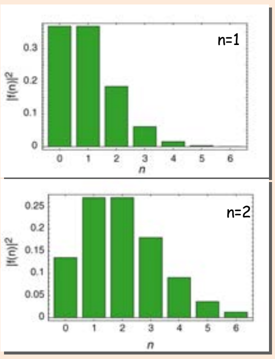

Mott-Insulator

Interaction energy dominsates

Atoms are completely localized to lattice sites !

$$|\Psi_{Mott}\rangle \propto \prod_{i=1}^{M}\left(a_i^\dagger\right)^n|0\rangle \qquad \langle a_i\rangle = 0$$

Fock states with vanishing atom number fluctuations

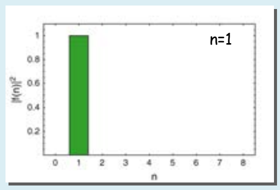

The Bose-Hubbard model
superfluid limit

$$H = -J\sum_{\langle i,j\rangle} \hat{a}_i^\dagger \hat{a}_j + \cancel{\frac{1}{2}U\sum_i \hat{n}_i(\hat{n}_i - 1)}$$

Atoms are delocalized over the entire lattice !
Macroscopic wave function φ_i describes this state very well.

$$|\Psi_{SF}\rangle \propto \left(\sum_{i=1}^{M} \hat{a}_i^\dagger\right)^N |0\rangle$$

$$\varphi_i = \langle \hat{a}_i \rangle; \quad |\Psi\rangle_i = e^{-|\varphi_i|^2/2} \sum_n \frac{\varphi_i^n}{\sqrt{n!}} |n\rangle$$

Atom number distribution after a measurement

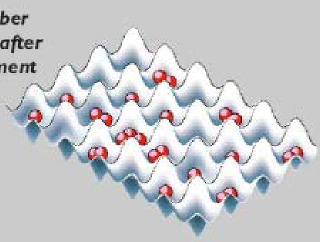

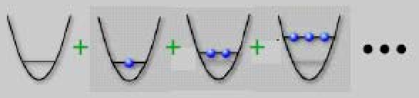

Coherent state with well defined macroscopic phase φ_i and poissonian atom number distribution at each lattice site

The Bose-Hubbard model
Mott-insulator limit

$$H = \cancel{-J\sum_{\langle i,j\rangle} \hat{a}_i^\dagger \hat{a}_j} + \frac{1}{2}U\sum_i \hat{n}_i(\hat{n}_i - 1)$$

MI ground state: Atoms are completely localized to lattice sites !

$$|\Psi_{Mott}\rangle \propto \prod_{i=1}^{M} \left(a_i^\dagger\right)^n |0\rangle$$

Fock states with vanishing atom-number fluctuation are formed.

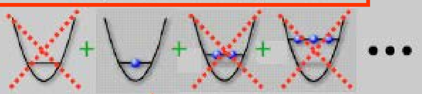

→ *no macroscopic phase*

$$\langle a_i \rangle = 0$$

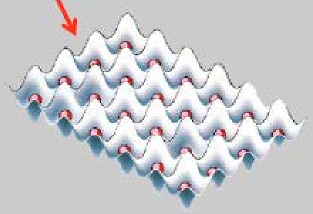

Proposal: Mott with BEC in 3D lattice:
D. Jaksch et al., PRL 81, 3108 (1998)

Quantum Phase Transition

Jaksch et al. PRL 81, 3108 (1998)

The Simplest Possible "Lattice": 2 Atoms in a Double Well

Superfluid State

$\frac{1}{\sqrt{2}}(\phi_l+\phi_r)\otimes\frac{1}{\sqrt{2}}(\phi_l+\phi_r)$

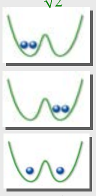

<n> = 1

$\langle E_{int}\rangle = \frac{1}{2}U$

Mott Ins. State

$\frac{1}{\sqrt{2}}\phi_l\otimes\phi_r+\frac{1}{\sqrt{2}}\phi_r\otimes\phi_l$

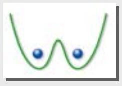

<n> = 1

$\langle E_{int}\rangle = 0$

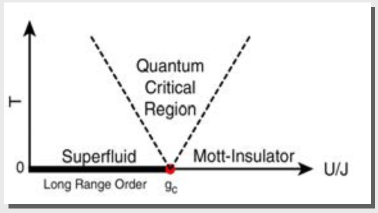

At the **critical point** g_c the system will undergo a phase transition from a superfluid to an insulator !

This phase transition occurs even at T=0 and is driven by quantum fluctuations !

Critical ratio for: U/J = 5.8

Characteristic for a QPT

- Excitation spectrum is dramatically modified at the critical point.
- U/J < g_c (Superfluid regime) Excitation spectrum is gapless
- U/J > g_c (Mott-Insulator regime) Excitation spectrum is gapped

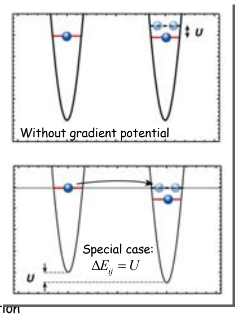

inhomogeneous system

effective local chemical potential

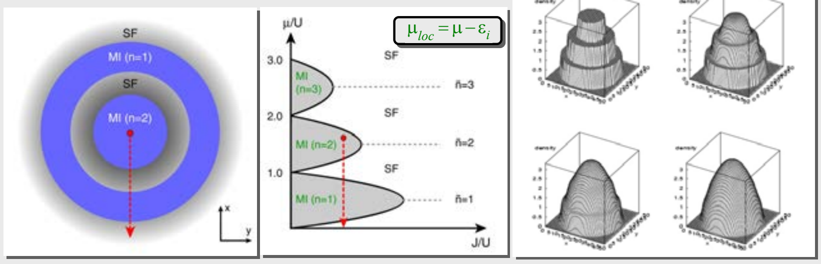

Quantum Phase Transition

M. Greiner et al. Nature **415**, p38 (2002)

Ramping up the Lattice Potential

Lattice Potential is increased

U/J reaches critical value

Phase Transition to a Mott-Insulator

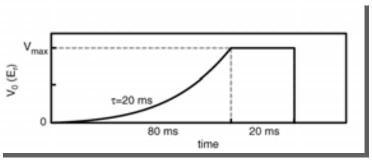

Momentum Distribution for Different Potential Depths

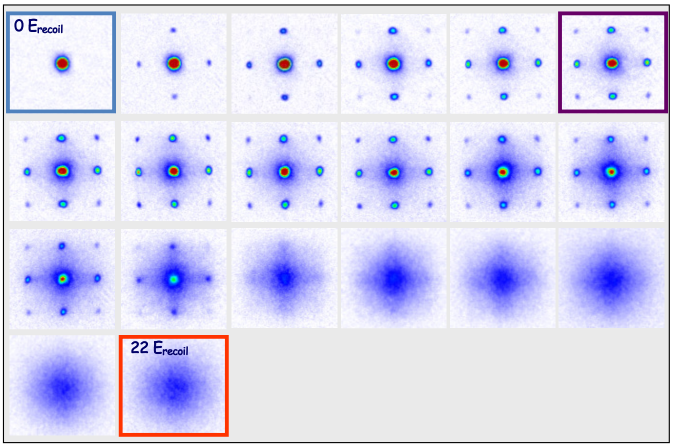

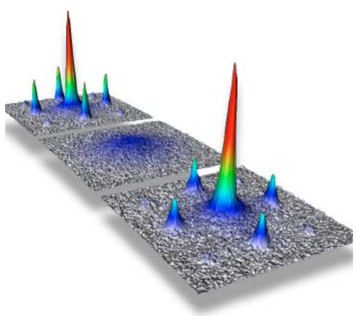

pure BEC
no lattice

superfluid in weak lattice
coherent point sources
interference

Localized atoms
no phase relation
between sites

measuring the MI exitation gap

the ultimate proof for the quantum phase transition: probing the excitation spectrum

there are many ways to loose and restore coherence:
Dalibard experiments questions Kesvich in 2004 by observing high contrast interference in 30 independent condensates
$\rightarrow$ interference is not neccesarily a proof for coherent / Fock state

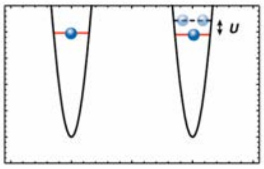

If one would apply a pertubation Δ to the system (e.g. shaking)

for atoms to hopping sites this costs interaction energy U

No excitations below threshold energy Δ=U

$\rightarrow$ gap in excitation spectrum

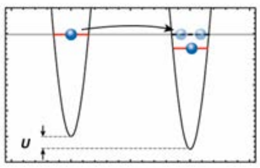

How can this be measured: apply a gradient:

If the gradient corresponds to the interaction energy, excitations are easily created

(actually, only applying the gradient is pertubation enough, tunneling is now allowed)

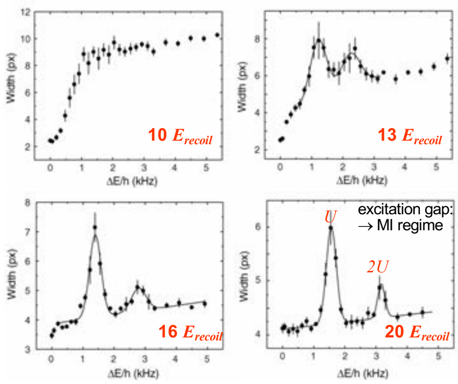

Collapse and Revival of Coherent States

$$|\alpha\rangle(t) = e^{-|\alpha|^2/2}\sum_n \frac{\alpha^n}{\sqrt{n!}} e^{-i\frac{1}{2}Un(n-1)t/\hbar}|n\rangle$$

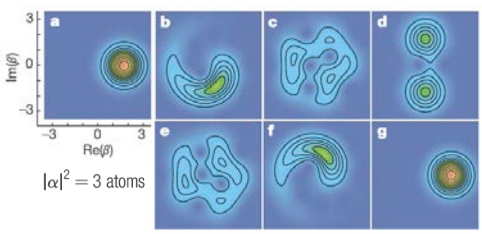

a, $t = 0\,h/U$; **b**, 0.1 h/U; **c**, 0.4 h/U **d**, 0.5 h/U; **e**, 0.6 h/U; **f**, 0.9 h/U; and **g**, h/U.

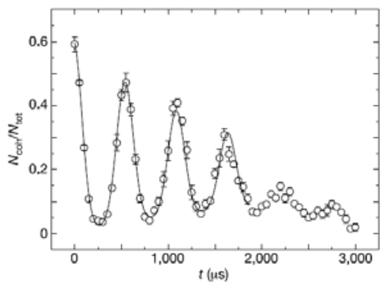

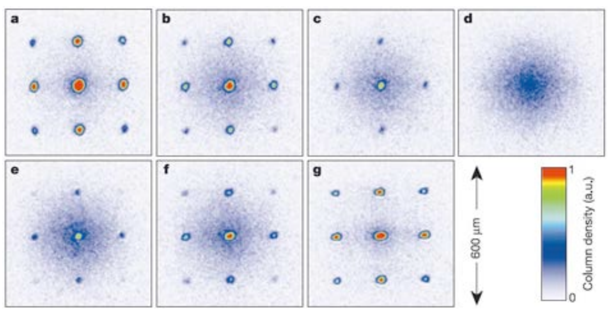

a, 0 μs; **b**, 100 μs; **c**, 150 μs; **d**, 250 μs; **e**, 350 μs; **f**, 400 μs; and **g**, 550 μs.

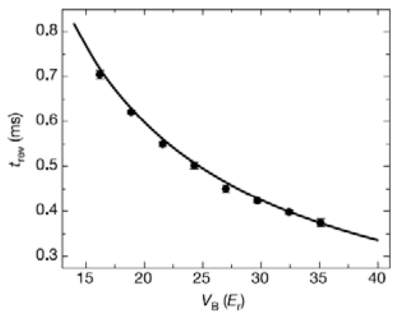

Measuring the populatipon
adiabatic switching off the lattice

Crystal momentum

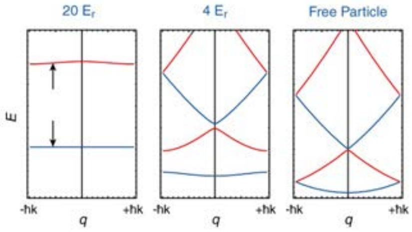

By adiabatic switching off the lattice:
Population of nth band is mapped onto nth Brillouin zone !

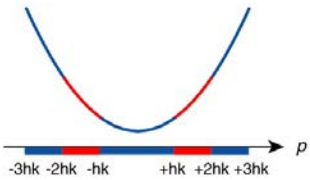

Momentum distribution of a dephased condensate
after turning off the lattice potential adiabtically

Brillouin Zones in 2D

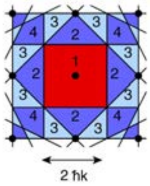

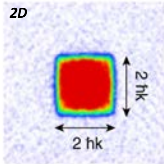

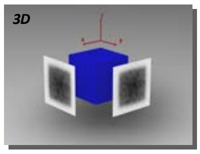

Populating higher energy bands
stimulated Raman transitions

Single lattice site

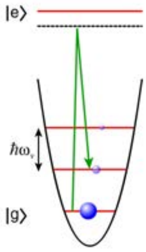

Energy bands

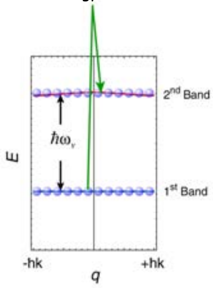

Experiment

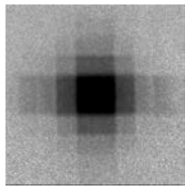

A. Kastberg et al. PRL 74, 1542 (1995)
M. Greiner et al. PRL 87, 160405 (2001)

Measuring the populatipon
adiabatic switching off the lattice

so far, this has been „single particle physics with many particles“,
it doesn‘t need a BEC, not even bosons:

releasing ground state atoms from the same optical lattice:

^{87}Rb

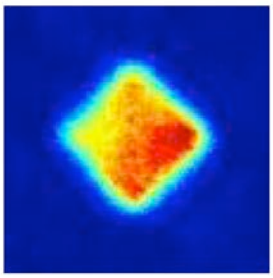

bosons

^{40}K

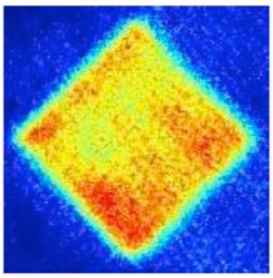

fermions

difference in momentum is only due to different masses

Study Order by higher order Correlations Quantum Noise Interferometry

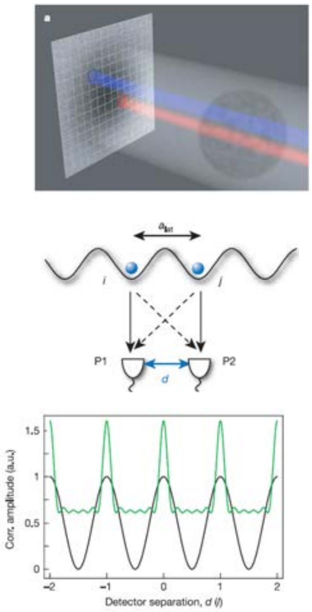

normalized density–density correlation function:

$$C(\mathbf{d}) = \frac{\int \langle n(\mathbf{x}+\mathbf{d}/2)\cdot n(\mathbf{x}-\mathbf{d}/2)\rangle d^2\mathbf{x}}{\int \langle n(\mathbf{x}+\mathbf{d}/2)\rangle \langle n(\mathbf{x}-\mathbf{d}/2)\rangle d^2\mathbf{x}}$$

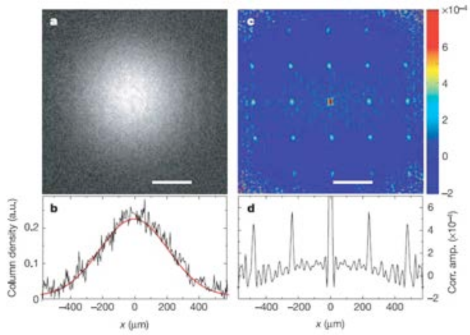

Quantum Noise Interferometry Fermions in a Lattice

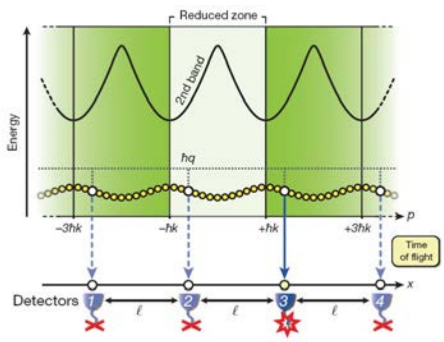

Figure 1 | Origin of anticorrelations in a Fermi gas released from an optical lattice. Each occupied Bloch state, labelled by a crystal momentum $\hbar q$, is represented by a dot in the reduced zone scheme (white region). The full occupation of the lowest energy band opposed to the empty second band describes the fermionic band insulating state. The periodically extended zone scheme (extension shown as green shaded region) shows that each Bloch state is a superposition of states with momenta equally spaced by $2\hbar k$. After the lattice is switched off abruptly, an atom with crystal momentum $\hbar q$ propagates freely during a time of flight t and can reach detectors equally spaced by a distance ℓ. If for example, detector number 3 detects a particle (yellow dot above detector), then owing to the single occupancy of each Bloch state dictated by the Pauli principle, detectors 1, 2 and 4 will not detect a particle (white dots above detectors).

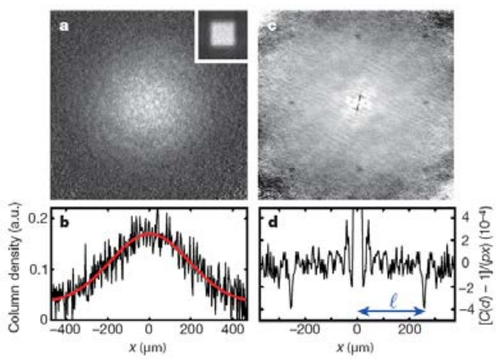

Figure 2 | Single shot absorption images and correlation analysis. a, Single absorption image of a fermionic ^{40}K atom cloud after 10 ms of free expansion. The inset shows a Brillouin zone mapping of the cloud, demonstrating that the Fermi gas is in a band insulating state. **b,** One-dimensional cut through **a** together with a gaussian fit (red). **c,** Spatial noise correlations obtained from an analysis of 158 independent images, showing an array of eight dark dots. **d,** A horizontal profile through the centre of the image shows that these dots correspond to correlation dips, with the characteristic spacing ℓ. The profile has been high-pass filtered to suppress a broad gaussian background that we attribute to shot to shot fluctuations in the atom number.

Quantum Gas Microscope
detecting single atoms in lattice

Quantum Gas Microscope
detecting single atoms in lattice

W. S. Bakr et al., nature **462**, 74 (2009)

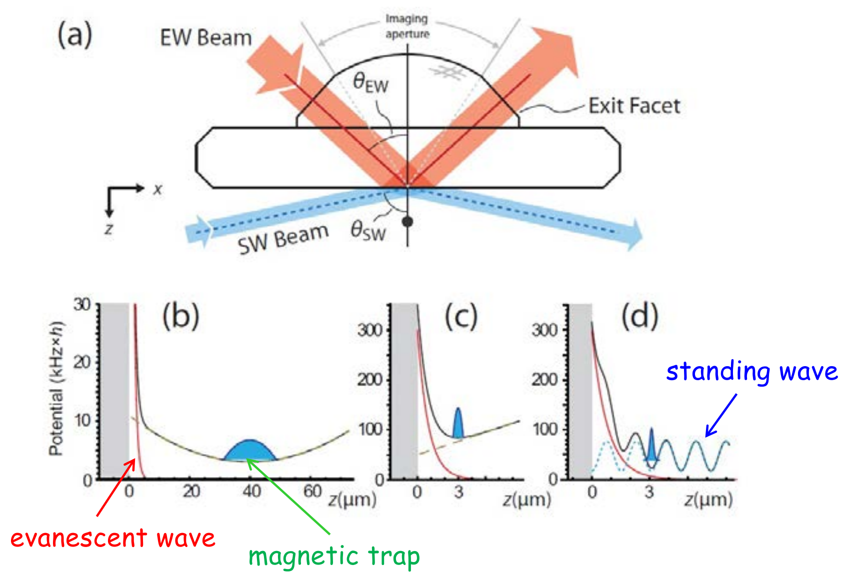

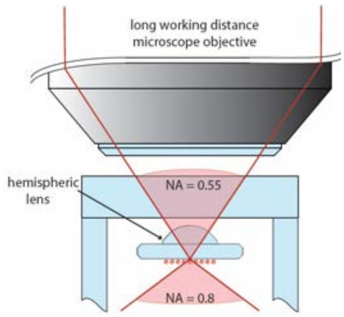

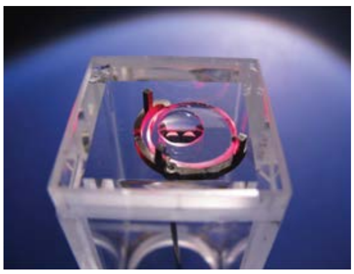

Quantum Gas Microscope
detecting single atoms in lattice

W. S. Bakr et al., nature **462**, 74 (2009)

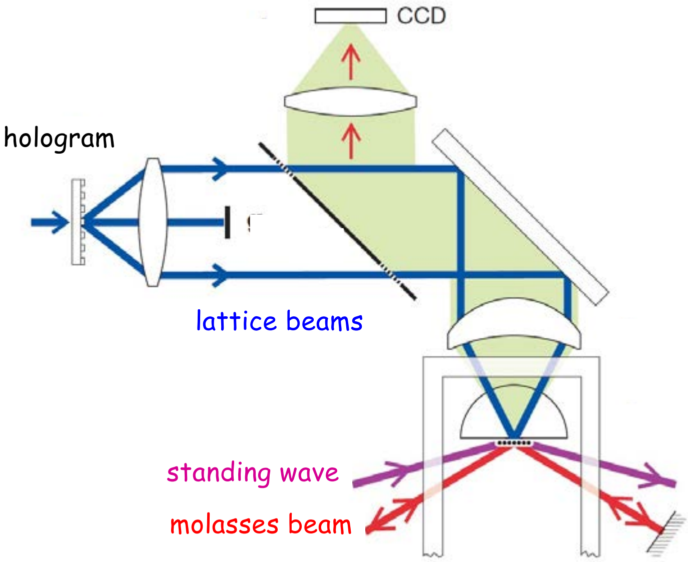

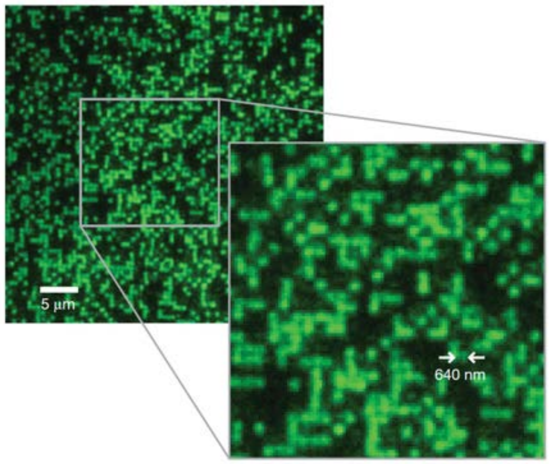

Quantum Gas Microscope
Mott Insulator

W. S. Bakr et al., Science **329**, 547 (2010)

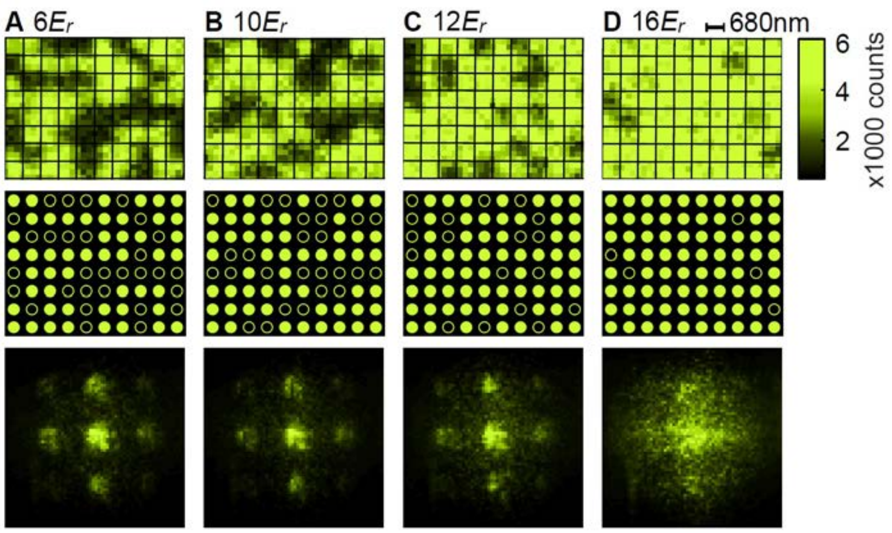

Mott shells

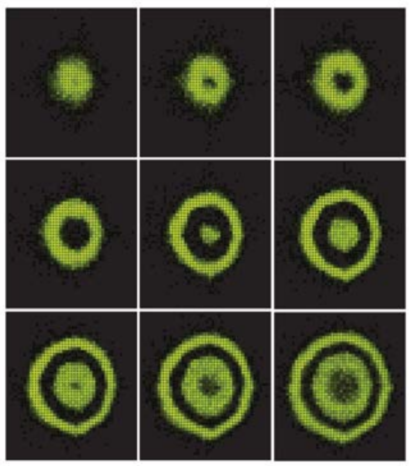

increasing atom number
averaged images

Quantum Gas Microscope
detecting single atoms in lattice

Christof Weitenberg, thesis
Bloch group @ MPQ

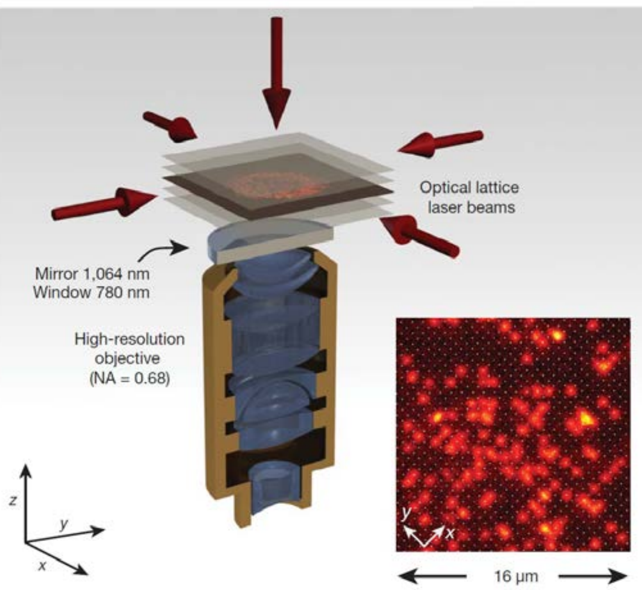

Selection of single 2D plane

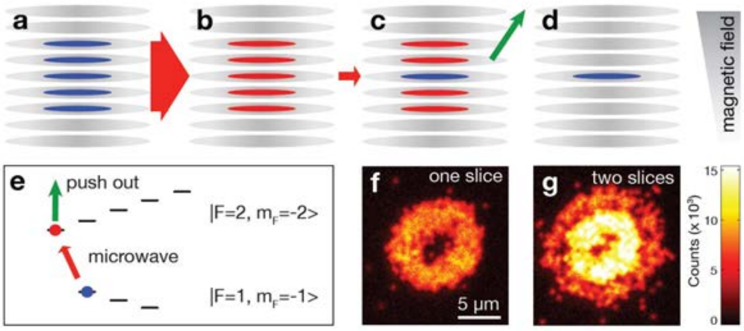

Quantum Gas Microscope
Mott Insulator

J. F. Sherson, nature, **467**, 68 (2010)

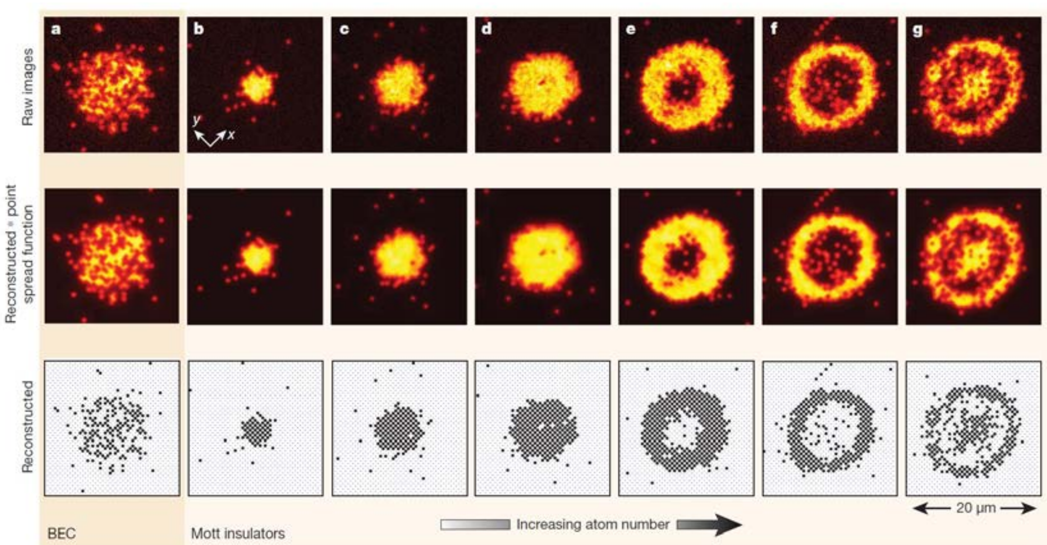

What can they probe?

- **Ground state** problems
  - Hubbard model, probing high-Tc superconductivity

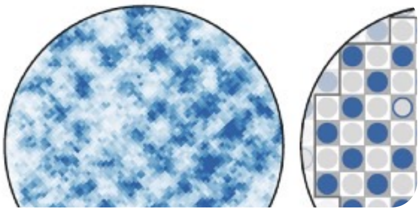

  - Cooled to create a magnetic state with long-range order

Mazurenko, Chiu, Ji, Parsons, Kanász-Nagy, Schmidt, Grusdt, Demler, Greif, Greiner, Nature 545, 462 (2017)
Esslinger, Ann Rev Cond Mat Phys 1, 129 2010

  - Many-body localization (1D-2D)

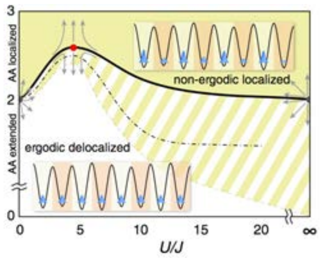

  - Debated in 2D

Schreiber, Hodgman, Bordia, Lüschen, Fischer, Vosk, Altman, Schneider, Bloch, Science 349, 842 (2015)

Artificial gauge fields

By rotation

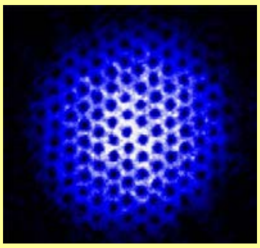

The Quantum Hall effect

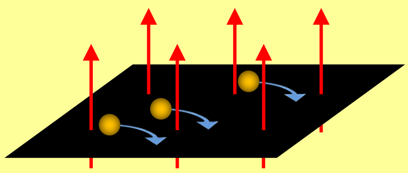

By Raman coupling in bulk

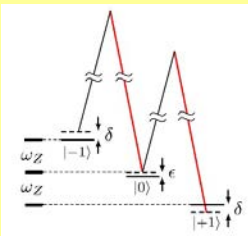

By Raman coupling in lattice

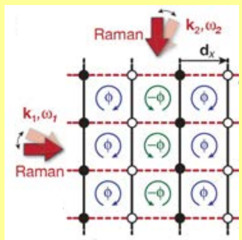

Digital Quantum Simulation

Lloyd, S. *Universal quantum simulators*. Science 273, 1073 (1996)

In 1996 S. Lloyd, showed that quantum simulation can be performed with arbitrary precision in polynomial time, using a Trotter-Suzuki's decomposition of the many-body evolution operator into sequences of local Hamiltonian evolutions. This can be then implemented by sequence of elementary quantum gates.

Example:

- *Universal digital quantum simulation with trapped ions*, B. P. Lanyon, et al., Science **334**, 57 (2011)
- *Real-time dynamics of lattice gauge theories with a few-qubit quantum computer*, E. A. Martinez et al. Nature **534**, 516 (2016)

What is the error accumulated by the 'Trotterisation'?

Quantum localization bounds Trotter errors in digital quantum simulation
M. Heyl, P. Hauke, P. Zoller Science Advances **5**:eaau8342 (2019)

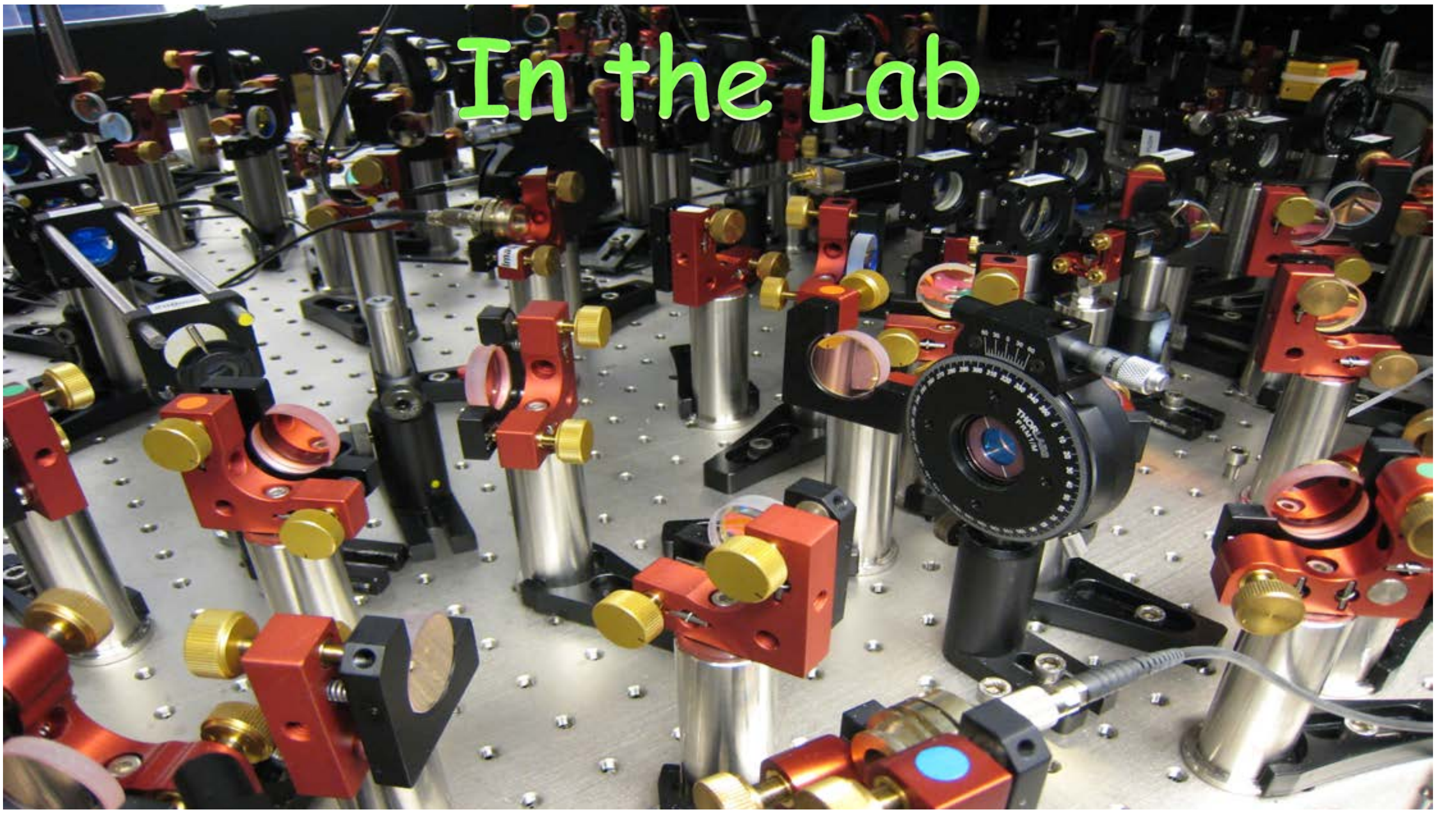

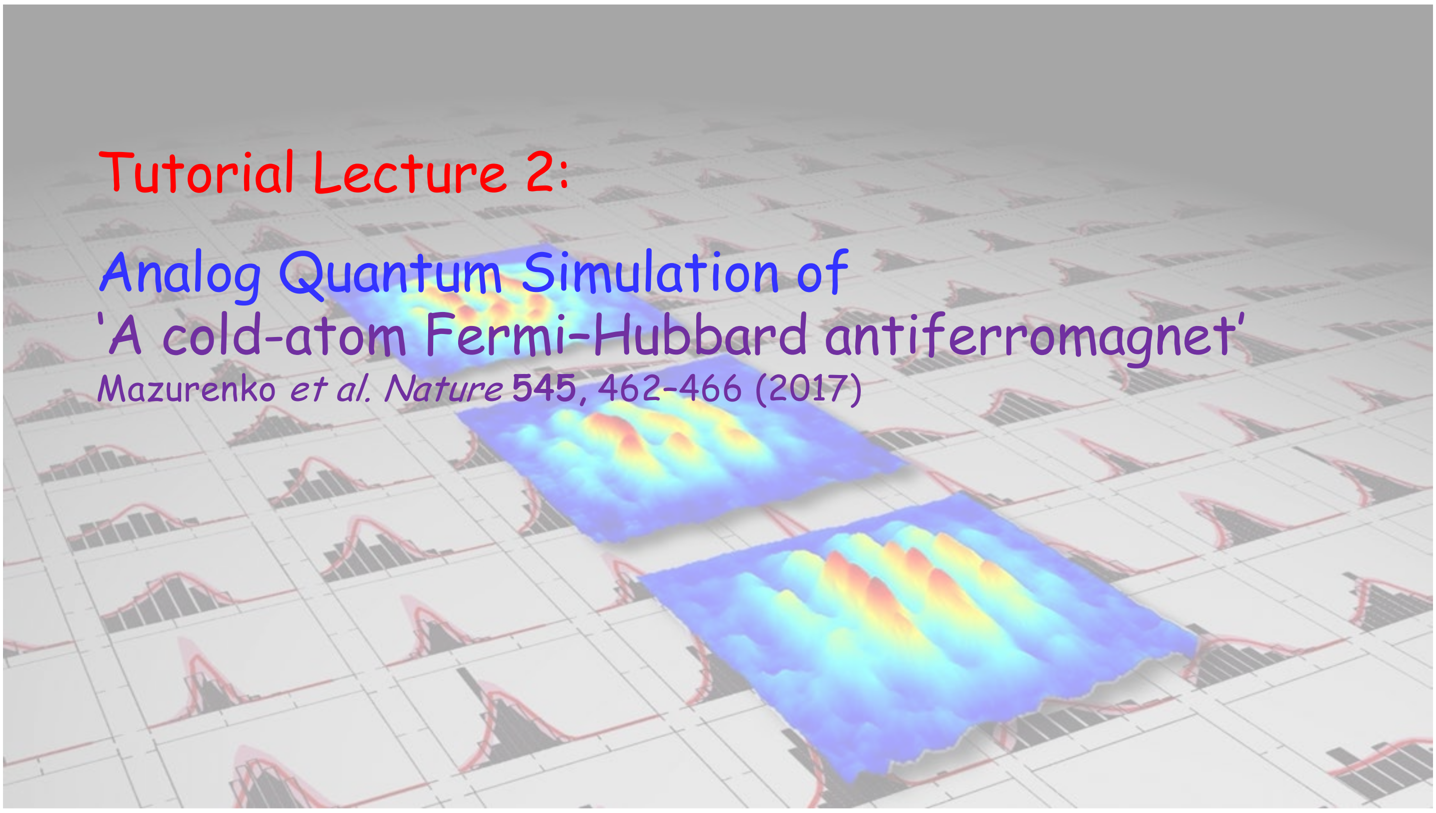

Tutorial Lecture 2:

Analog Quantum Simulation of
'A cold-atom Fermi-Hubbard antiferromagnet'

Mazurenko *et al.* *Nature* **545**, 462-466 (2017)

A cold-atom Fermi-Hubbard antiferromagnet

Nature **545**, 462-466 (2017)

Exotic phenomena in systems with strongly correlated electrons emerge from the interplay between spin and motional degrees of freedom. For example, doping an antiferromagnet is expected to give rise to pseudogap states and high-temperature superconductors[1]. Quantum simulation[2,3,4,5,6,7,8] using ultracold fermions in optical lattices could help to answer open questions about the doped Hubbard Hamiltonian[9,10,11,12,13,14], and has recently been advanced by quantum gas microscopy[15,16,17,18,19,20]. Here we report the realization of an antiferromagnet in a repulsively interacting Fermi gas on a two-dimensional square lattice of about 80 sites at a temperature of 0.25 times the tunnelling energy. The antiferromagnetic long-range order manifests through the divergence of the correlation length, which reaches the size of the system, the development of a peak in the spin structure factor and a staggered magnetization that is close to the ground-state value. We hole-dope the system away from half-filling, towards a regime in which complex many-body states are expected, and find that strong magnetic correlations persist at the antiferromagnetic ordering vector up to dopings of about 15 per cent. In this regime, numerical simulations are challenging[21] and so experiments provide a valuable benchmark. Our results demonstrate that microscopy of cold atoms in optical lattices can help us to understand the low-temperature Fermi–Hubbard model.

Probing antiferromagnetism in the Hubbard model with a quantum gas microscope

A Mazurenko *et al.* *Nature* **545**, 462–466 (2017)
doi:10.1038/nature22362

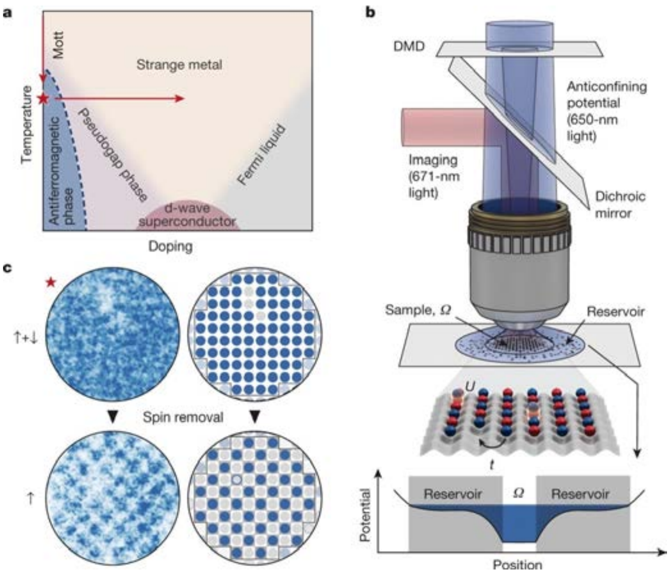

Figure 1 | Probing antiferromagnetism in the Hubbard model with a quantum gas microscope. a, Schematic of the two-dimensional Hubbard phase diagram, including predicted phases. We explore the trajectories traced by the red arrows for a Hubbard model with $U/t = 7.2(2)$. The strongest antiferromagnetic order is observed at the starred point. **b,** Experimental set-up. We trap ^{6}Li atoms in a two-dimensional square optical lattice. We use the combined potential of the optical lattice and the anticonfinement that is generated by the digital micromirror device (DMD) to trap the atoms in a central sample Ω of homogeneous density, surrounded by a dilute reservoir, as shown in the plot. The system is imaged with 671-nm light along the same beam path as the projected 650-nm potential, and separated from it by a dichroic mirror. **c,** Exemplary raw (left) and processed (right) images of the atomic distribution of single experimental realizations, with both spin components present (upper; corresponding to the starred point in **a**) and with one spin component removed (lower). The observed chequerboard pattern in the spin-removed images indicates the presence of an antiferromagnet.

Observing antiferromagnetic long-range order

A Mazurenko *et al.* *Nature* **545**, 462–466 (2017)
doi:10.1038/nature22362

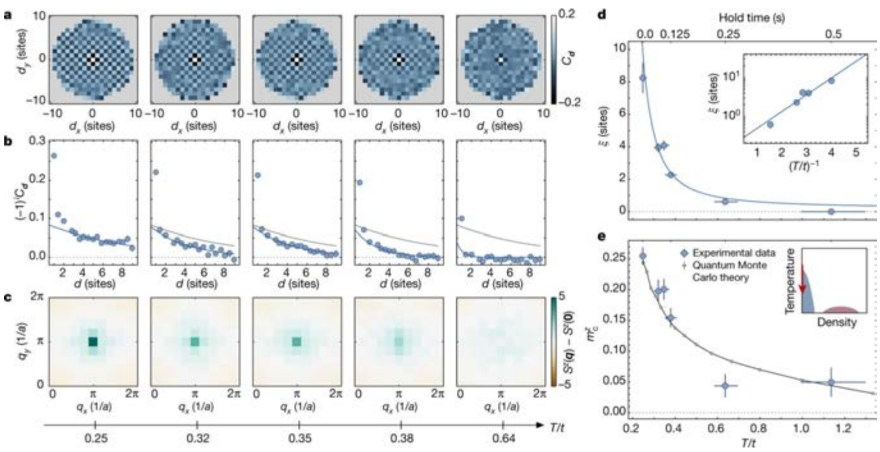

Figure 2 | Observing antiferromagnetic long-range order. a, The spin correlator C_d is plotted for different displacements $\mathbf{d} = (d_x, d_y)$ ranging across the entire sample for five temperatures T/t. We record more than 200 images for each temperature (Methods). Correlations extend across the entire sample for the coldest temperatures, whereas for the hottest temperature only nearest-neighbour correlations remain. **b,** The sign-corrected correlation function $(-1)^i C_d$ is obtained through an azimuthal average. The exponential fits to the data ($|\mathbf{d}| = d > 2$ sites) are shown in blue, from which we determine the correlation length ξ; the fit of the coldest sample is plotted in grey in the other panels for comparison. **c,** The measured spin structure factor $S^z(\mathbf{q}) - S^z(\mathbf{0})$ obtained from Fourier transformations of single images. A peak at momentum $\mathbf{q}_{\mathrm{AFM}} = (\pi/a, \pi/a)$ signals the presence of an antiferromagnet. **d,** The measured correlation length ξ (data), fitted to equation (2) (curve), diverges exponentially as a function of temperature T/t and is comparable to the system size for the lowest temperature. The temperature is varied by holding the atoms in the trap for a variable time. The inset is a semi-logarithmic plot of the same quantity versus inverse temperature. **e,** The measured corrected staggered magnetization m_c^z (large blue circles) increases markedly below temperatures $T/t \approx 0.4$. We find good agreement with quantum Monte Carlo calculations of the Hubbard model (small grey circles). The trajectory followed in this figure is shown schematically in the phase diagram in the inset. Error bars in **d** and **e** are standard deviations of the sampled mean; error bars in **b** (smaller than the markers) are computed as in Methods. The figure is based on 2,282 experimental realizations.

Full counting statistics of the staggered magnetization operator

A Mazurenko *et al.* *Nature* **545**, 462–466 (2017)
doi:10.1038/nature22362

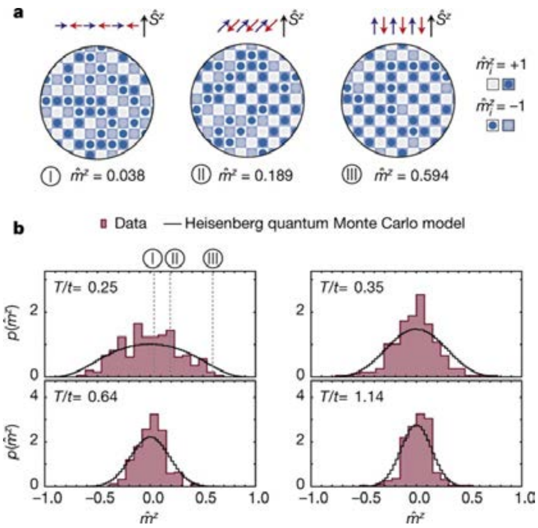

Figure 3 | Full counting statistics of the staggered magnetization operator. a, Selected images with one spin component removed (chequerboard overlaid to guide the eye) show a large variation in ordering strength at the coldest temperature. This variation is a consequence of the SU(2) symmetry of the underlying Hamiltonian, which leads to different orientations of the staggered spin-ordering vector $\hat{\boldsymbol{m}}$ relative to the measurement axis z, as shown schematically by the spin vectors (red and blue arrows) relative to the axis defined by $\hat{S}^z$ (black arrows). **b**, Measured distributions of the staggered magnetization operator, $p(\hat{m}_z)$, are plotted at different temperatures T/t (histograms). We find excellent agreement with quantum Monte Carlo simulations of the Heisenberg model with no free fitting parameters (black lines). The figure is based on 2,282 experimental realizations.

Doping the antiferromagnet

A Mazurenko *et al.* *Nature* **545**, 462–466 (2017)
doi:10.1038/nature22362

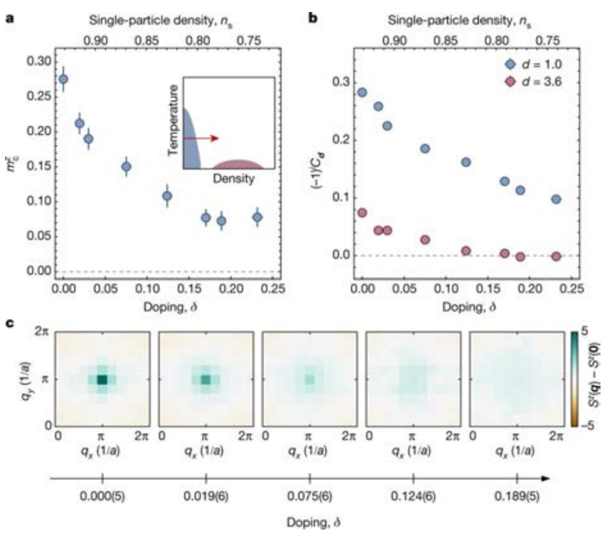

Figure 4 | Doping the antiferromagnet. a, We dope the system with holes and reduce the density from half-filling, with $0.0 \leq \delta \leq 0.25$ (corresponding to $0.95 \geq n_s \geq 0.73$). The corrected staggered magnetization m_c^z settles at the critical hole doping $\delta_c \approx 0.15$. The trajectory followed in this figure is shown schematically in the phase diagram in the inset. **b**, The relative strength of the sign-corrected spin correlations $(-1)^i C_d$ decreases less rapidly with hole doping at smaller distances ($d = 1.0$) than at larger distances ($d = 3.6$). For large doping, only the nearest-neighbour correlator is appreciable, so this correlation is predominantly responsible for the non-zero staggered magnetization away from the antiferromagnetic phase. **c**, We show the spin structure factor $S^z(\boldsymbol{q}) - S^z(\boldsymbol{0})$, as in Fig. 2c, for each doping value. Error bars in **a** are standard deviations of the sampled mean; those in **b** are computed as in Methods. The figure is based on 1,470 experimental realizations.